

Score-Based Turbo Message Passing for Plug-and-Play Compressive Image Recovery*

Chang Cai¹, Xiaojun Yuan², and Ying-Jun Angela Zhang¹

¹Department of Information Engineering, The Chinese University of Hong Kong

²National Key Lab. of Wireless Commun., University of Electronic Science and Technology of China

Abstract

Message passing algorithms have been tailored for compressive imaging applications by plugging in different types of off-the-shelf image denoisers. These off-the-shelf denoisers mostly rely on some generic or hand-crafted priors for denoising. Due to their insufficient accuracy in capturing the true image prior, these methods often fail to produce satisfactory results, especially in largely underdetermined scenarios. On the other hand, score-based generative modeling offers a promising way to accurately characterize the sophisticated image distribution. In this paper, by exploiting the close relation between score-based modeling and empirical Bayes-optimal denoising, we devise a message passing framework that integrates a score-based minimum mean squared error (MMSE) denoiser for compressive image recovery. This framework is firmly rooted in Bayesian formalism, in which state evolution (SE) equations accurately predict its asymptotic performance. Experiments on the FFHQ dataset demonstrate that our method strikes a significantly better performance-complexity tradeoff than conventional message passing, regularized linear regression, and score-based posterior sampling baselines. Remarkably, our method typically requires less than 20 neural function evaluations (NFEs) to converge.

Keywords: Message passing, score-based generative models, plug-and-play priors, linear inverse problems

1 Introduction

Consider the problem of recovering an image $\mathbf{x} \in \mathbb{R}^N$ from noisy linear measurements $\mathbf{y} \in \mathbb{R}^M$ of the form

$$\mathbf{y} = \mathbf{A}\mathbf{x} + \mathbf{n}, \quad (1)$$

where $\mathbf{A} \in \mathbb{R}^{M \times N}$ is a known measurement matrix, and $\mathbf{n} \in \mathbb{R}^M$ is an additive white Gaussian noise (AWGN) with zero mean and covariance $\delta_0^2 \mathbf{I}$. This problem arises in different imaging domains,

*Emails: cc021@ie.cuhk.edu.hk; xjyuan@uestc.edu.cn; yjzhang@ie.cuhk.edu.hk.

such as magnetic resonance imaging, synthetic aperture radar, and computed tomography. In these applications, it is often the case of $M \ll N$, making the linear inverse problem underdetermined. Therefore, it is essential to incorporate prior knowledge of \mathbf{x} into the estimation process. This problem is broadly referred to as *compressive image recovery* in the literature [24].

Inspired by belief propagation (BP) in graphical models, message passing algorithms stand as a powerful tool for Bayesian compressive sensing (CS), enabling the incorporation of a variety of sparsity-inducing priors. To name a few, approximate message passing (AMP) [9] utilizes a quadratic approximation of max-sum loopy BP to efficiently implement the least absolute shrinkage and selection operator (LASSO). The LASSO solution is equivalent to the maximum *a posteriori* (MAP) estimator assuming a Laplacian prior. Turbo-CS [21], also known as vector approximate message passing (VAMP) [25], employs a Bernoulli-Gaussian distribution for modeling the sparsity pattern. Please refer to [37] for a comprehensive review of other variants of message passing algorithms.

Unfortunately, sparsity-based approaches often exhibit poor performance in many imaging applications. The reason is that natural images do not have an exact sparse representation in any known transform domain (e.g., discrete cosine transform (DCT), wavelet, curvelet). To address this limitation, off-the-shelf image denoisers have been plugged into message passing algorithms for performance enhancement [24, 27, 34]. Popular choices include the total variation (TV) denoiser, the SURE-LET denoiser [3], the BM3D denoiser [7], etc. These off-the-shelf denoisers mostly rely on non-parametric models for denoising, which do not require the hypothesis of a statistical model for the noiseless image. Consequently, the above-mentioned plug-and-play methods can result in sub-optimal performance, as they fail to fully exploit the strong prior inherent in image data. Some recent works [23, 32] also incorporate either a denoising CNN (DnCNN) or an unrolled network in place of the off-the-shelf denoiser.

On the other hand, score-based generative models [29, 15, 30] have achieved unparalleled success in generating high-quality samples across various domains, including images, videos, and molecular conformations. This evidences their remarkable capabilities in capturing the intricacies of high-dimensional data distribution. During training, score-based generative models perturb the data with random Gaussian noise of different magnitudes. They learn the data prior by matching the gradient of the log density of the perturbed data, known as *score function*. The score function is then applied at each and every reverse diffusion step for sample generation.

The score-based generative models can also be leveraged for solving inverse problems without task-specific training [17, 18, 5, 6, 28, 36, 10]. These methods obtain a prior-related term (i.e., the score function) from the score-based generative network and a likelihood term from the degradation model. The two terms are combined to form the posterior term via Bayes' theorem, enabling solving inverse problems stochastically by sampling from the posterior distribution. However, these methods typically require traversing the entire reverse diffusion process, necessitating hundreds or even thousands of neural function evaluations (NFEs), which makes them computationally expensive. Moreover, sampling from the exact posterior distribution is indeed intractable due to the time dependence of the likelihood. This challenge has led to various approximations used in posterior sampling, typically achieved through projection at each time step to enforce data consistency [5], or

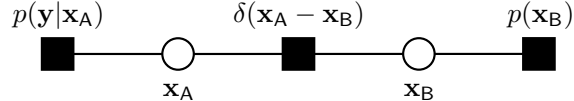


Figure 1: Factor graph for Turbo-CS derivation. The circles represent variable nodes and the squares represent factor nodes.

a reweighted combination of the prior score and the estimated likelihood function [6]. Please refer to a recent survey paper [8] for different categories of approximations. These approximations often introduce additional hyperparameters that are sensitive and require careful tuning. Furthermore, the approximation errors accumulate through successive iterations, making it challenging to assess their performance theoretically.

In this paper, we devise a score-based message passing algorithm for compressive imaging within the Bayesian framework. This approach inherits the fast convergence speed of message passing and, meanwhile, fully leverages the image prior through the integration of score-based networks. We exploit the fact that, at each iteration, message passing algorithms construct a pseudo AWGN observation of the ground-truth image. We repurpose the score function for denoising the AWGN observation through Tweedie’s formula [11], achieving per-iteration minimum mean squared error (MMSE) performance with a single forward pass through the score-based network. This significantly differs from the typical usage of the score function for reverse diffusion sampling. We further relate the posterior variance calculation to the second-order generalization of Tweedie’s formula, which depends on the Hessian of the log density (i.e., the second-order score function) [22]. We propose matching the second-order score function to obtain the posterior variance, facilitating message updates in a turbo-type message passing algorithm. This approach leads to the name *score-based turbo message passing* (STMP). We present the state evolution (SE) analysis to track the asymptotic MSE performance of STMP. Experimental results on the FFHQ dataset [16] demonstrate that STMP strikes a much better tradeoff between performance and complexity than existing conventional message passing, regularized linear regression, and score-based posterior sampling schemes. Notably, STMP typically requires less than 20 NFEs to converge.

2 Turbo-CS Framework

In this section, we review the Turbo-CS framework [21, 25] based on an expectation-propagation (EP) type message-passing derivation on the factor graph.

The posterior distribution can be factorized as

$$p(\mathbf{x}|\mathbf{y}) \propto p(\mathbf{x})p(\mathbf{y}|\mathbf{x}). \quad (2)$$

By letting $\mathbf{x}_A = \mathbf{x}_B = \mathbf{x}$, we obtain an equivalent factorization of (2):

$$p(\mathbf{x}_A, \mathbf{x}_B|\mathbf{y}) \propto p(\mathbf{x}_B)\delta(\mathbf{x}_A - \mathbf{x}_B)p(\mathbf{y}|\mathbf{x}_A), \quad (3)$$

Algorithm 1 Turbo-CS Framework

```

1: Input:  $\mathbf{A}$ ,  $\mathbf{y}$ ,  $\delta_0^2$ ,  $\mathbf{x}_A^{pri}$ ,  $v_A^{pri}$ 
2: Output:  $\mathbf{x}_B^{post}$ 
3: repeat
4:   % LMMSE estimator
5:    $\mathbf{x}_A^{post} = \mathbf{x}_A^{pri} + v_A^{pri} \mathbf{A}^\top (v_A^{pri} \mathbf{A} \mathbf{A}^\top + \delta_0^2 \mathbf{I})^{-1} (\mathbf{y} - \mathbf{A} \mathbf{x}_A^{pri})$ 
6:    $v_A^{post} = v_A^{pri} - \frac{(v_A^{pri})^2}{N} \text{tr}(\mathbf{A}^\top (v_A^{pri} \mathbf{A} \mathbf{A}^\top + \delta_0^2 \mathbf{I})^{-1} \mathbf{A})$ 
7:    $v_A^{ext} = 1 / (1/v_A^{post} - 1/v_A^{pri})$ 
8:    $\mathbf{x}_A^{ext} = v_A^{ext} (\mathbf{x}_A^{post} / v_A^{post} - \mathbf{x}_A^{pri} / v_A^{pri})$ 
9:    $\mathbf{x}_B^{pri} = \mathbf{x}_A^{ext}$ ,  $v_B^{pri} = v_A^{ext}$ 
10:  % MMSE denoiser
11:   $\mathbf{x}_B^{post} = \mathbb{E}[\mathbf{x}_B | \mathbf{x}_B^{pri}]$ 
12:   $v_B^{post} = \frac{1}{N} \text{tr}(\text{Cov}[\mathbf{x}_B | \mathbf{x}_B^{pri}])$ 
13:   $v_B^{ext} = 1 / (1/v_B^{post} - 1/v_B^{pri})$ 
14:   $\mathbf{x}_B^{ext} = v_B^{ext} (\mathbf{x}_B^{post} / v_B^{post} - \mathbf{x}_B^{pri} / v_B^{pri})$ 
15:   $\mathbf{x}_A^{pri} = \mathbf{x}_B^{ext}$ ,  $v_A^{pri} = v_B^{ext}$ 
16: until the stopping criterion is met

```

where $\delta(\cdot)$ is the Dirac delta function. The corresponding factor graph representation is shown in Fig. 1.

We start by initializing the message from the factor node $\delta(\mathbf{x}_A - \mathbf{x}_B)$ to the variable node \mathbf{x}_A as $\mu_{\delta \rightarrow \mathbf{A}}(\mathbf{x}_A) = \mathcal{N}(\mathbf{x}_A; \mathbf{x}_A^{pri}, v_A^{pri} \mathbf{I})$. According to the EP approximation, the belief on \mathbf{x}_A (i.e., the marginal posterior density estimate of \mathbf{x}_A) is given by $b(\mathbf{x}_A) = \mathcal{N}(\mathbf{x}_A; \mathbf{x}_A^{post}, \mathbf{V}_A^{post}) = \text{proj}[p(\mathbf{y} | \mathbf{x}_A) \mu_{\delta \rightarrow \mathbf{A}}(\mathbf{x}_A)]$, where $\text{proj}[p(\cdot)]$ denotes the projection of $p(\cdot)$ to a Gaussian probability density function (PDF) with matched first- and second-order moments. By noting that the product of two Gaussian messages is proportional to a Gaussian PDF, the projection operator in $b(\mathbf{x}_A)$ can thus be removed. We further approximate \mathbf{V}_A^{post} using a shared scalar variance [21, 25], resulting in the belief of the form $b(\mathbf{x}_A) \approx \mathcal{N}(\mathbf{x}_A; \mathbf{x}_A^{post}, v_A^{post} \mathbf{I})$, where

$$\mathbf{x}_A^{post} = \mathbf{x}_A^{pri} + v_A^{pri} \mathbf{A}^\top (v_A^{pri} \mathbf{A} \mathbf{A}^\top + \delta_0^2 \mathbf{I})^{-1} (\mathbf{y} - \mathbf{A} \mathbf{x}_A^{pri}), \quad (4)$$

$$v_A^{post} = v_A^{pri} - \frac{(v_A^{pri})^2}{N} \text{tr}(\mathbf{A}^\top (v_A^{pri} \mathbf{A} \mathbf{A}^\top + \delta_0^2 \mathbf{I})^{-1} \mathbf{A}). \quad (5)$$

Eqns. (4) and (5) are respectively the posterior mean and variance from the linear minimum mean-square error (LMMSE) estimator of \mathbf{x}_A , given the prior mean \mathbf{x}_A^{pri} and variance v_A^{pri} . The message from the variable node \mathbf{x}_A to the factor node $\delta(\mathbf{x}_A - \mathbf{x}_B)$, also known as the extrinsic message, is calculated as $\mu_{\mathbf{A} \rightarrow \delta}(\mathbf{x}_A) = \mathcal{N}(\mathbf{x}_A; \mathbf{x}_A^{ext}, v_A^{ext} \mathbf{I}) = \mathcal{N}(\mathbf{x}_A; \mathbf{x}_A^{post}, v_A^{post} \mathbf{I}) / \mathcal{N}(\mathbf{x}_A; \mathbf{x}_A^{pri}, v_A^{pri} \mathbf{I})$, yielding Lines 7 and 8 of Algorithm 1. The extrinsic message decorrelates the input and output estimation errors, i.e., $\mathbb{E}[(\mathbf{x}_A - \mathbf{x}_A^{pri})(\mathbf{x}_A - \mathbf{x}_A^{ext})^\top] = \mathbf{0}$ [20].

The message $\mu_{\mathbf{A} \rightarrow \delta}(\mathbf{x}_A) = \mathcal{N}(\mathbf{x}_A; \mathbf{x}_A^{ext}, v_A^{ext} \mathbf{I})$ flows rightward through the factor node $\delta(\mathbf{x}_A - \mathbf{x}_B)$ unchanged, manifesting as $\mu_{\delta \rightarrow \mathbf{B}}(\mathbf{x}_B) = \mathcal{N}(\mathbf{x}_B; \mathbf{x}_B^{pri}, v_B^{pri} \mathbf{I})$ on the other side. This leads to Line 9

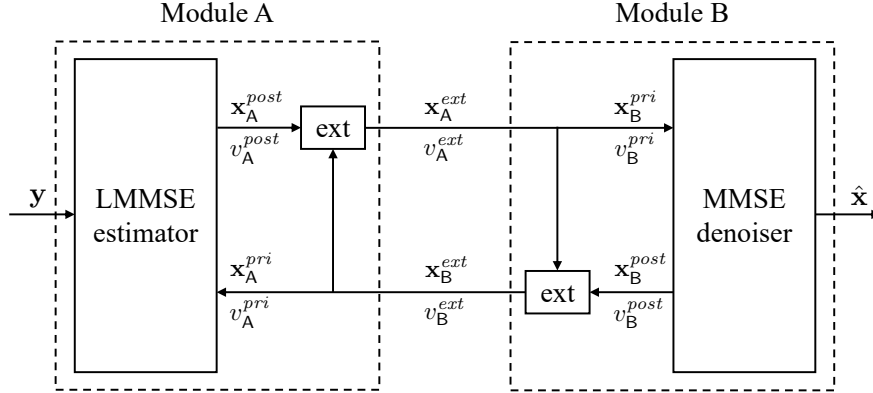


Figure 2: Modularized representation of the Turbo-CS algorithm.

of Algorithm 1. Then, based on the EP approximation, the belief on \mathbf{x}_B is calculated as $b(\mathbf{x}_B) = \mathcal{N}(\mathbf{x}_B; \mathbf{x}_B^{post}, \mathbf{V}_B^{post}) = \text{proj}[p(\mathbf{x}_B)\mu_{\delta \rightarrow B}(\mathbf{x}_B)]$, where

$$\mathbf{x}_B^{post} = \frac{1}{Z} \int_{\mathbf{x}_B} \mathbf{x}_B p(\mathbf{x}_B) \mathcal{N}(\mathbf{x}_B; \mathbf{x}_B^{pri}, v_B^{pri} \mathbf{I}), \quad (6)$$

$$\mathbf{V}_B^{post} = \frac{1}{Z} \int_{\mathbf{x}_B} (\mathbf{x}_B - \mathbf{x}_B^{pri})(\mathbf{x}_B - \mathbf{x}_B^{pri})^\top p(\mathbf{x}_B) \mathcal{N}(\mathbf{x}_B; \mathbf{x}_B^{pri}, v_B^{pri} \mathbf{I}), \quad (7)$$

with $Z = \int_{\mathbf{x}_B} p(\mathbf{x}_B) \mathcal{N}(\mathbf{x}_B; \mathbf{x}_B^{pri}, v_B^{pri} \mathbf{I})$ being the normalization constant. The state evolution (SE) analysis [13] has shown that the error vector $\mathbf{x}_B^{pri} - \mathbf{x}_B$ is asymptotically i.i.d. Gaussian as $M, N \rightarrow \infty$ with a fixed ratio. Based on this, the Turbo-CS algorithm models \mathbf{x}_B^{pri} as an AWGN observation of the true signal \mathbf{x}_B , i.e.,

$$\mathbf{x}_B^{pri} = \mathbf{x}_B + \mathbf{w}, \quad \mathbf{w} \sim \mathcal{N}(\mathbf{0}, v_B^{pri} \mathbf{I}). \quad (8)$$

From (8), we have $p(\mathbf{x}_B^{pri} | \mathbf{x}_B) = \mathcal{N}(\mathbf{x}_B^{pri}; \mathbf{x}_B, v_B^{pri} \mathbf{I})$. By noting that $\mathcal{N}(\mathbf{x}_B; \mathbf{x}_B^{pri}, v_B^{pri} \mathbf{I})$ in (6) and (7) takes the same form as $p(\mathbf{x}_B^{pri} | \mathbf{x}_B)$, the belief calculation on \mathbf{x}_B can be interpreted as the MMSE denoising under the AWGN observation model (8):

$$\mathbf{x}_B^{post} = \mathbb{E}[\mathbf{x}_B | \mathbf{x}_B^{pri}], \quad (9)$$

$$\mathbf{V}_B^{post} = \text{Cov}[\mathbf{x}_B | \mathbf{x}_B^{pri}]. \quad (10)$$

Similarly, we approximate \mathbf{V}_B^{post} by $v_B^{post} \mathbf{I}$ with $v_B^{post} = \frac{1}{N} \text{tr}(\text{Cov}[\mathbf{x}_B | \mathbf{x}_B^{pri}])$ to simplify calculation. The extrinsic message of \mathbf{x}_B is denoted as $\mu_{B \rightarrow \delta}(\mathbf{x}_B) = \mathcal{N}(\mathbf{x}_B; \mathbf{x}_B^{ext}, v_B^{ext} \mathbf{I})$, where the variance and mean are respectively given in Lines 13 and 14 of Algorithm 1. Finally, the extrinsic message of \mathbf{x}_B flows leftward through the factor node $\delta(\mathbf{x}_A - \mathbf{x}_B)$ unchanged, serving as the prior message of \mathbf{x}_B in the next iteration, i.e., $\mathbf{x}_A^{pri} = \mathbf{x}_B^{ext}, v_A^{pri} = v_B^{ext}$.

As illustrated in Fig. 2, the above message passing principle admits a modularized interpretation that resembles the turbo decoder [1], hence the name Turbo-CS. In particular, the Turbo-CS framework consists of two modules. Module A is a simplified LMMSE estimator of \mathbf{x} based on the

observation \mathbf{y} , in which the messages from module B serve as the prior mean and variance. With the equivalent AWGN observation model (8), Module B can be interpreted as an MMSE denoiser incorporating the prior distribution of \mathbf{x} and the messages from module A. The two modules are executed iteratively to refine the estimate of \mathbf{x} .

The main challenge in implementing the Turbo-CS algorithm arises from the MMSE denoising part in module B, primarily due to i) the lack of a tractable prior distribution and ii) the high-dimensional integrals involved in calculating the posterior mean and variance. To sidestep these difficulties, various off-the-shelf image denoisers (e.g., TV, SURE-LET [3], BM3D [7]) are plugged into message passing algorithms in place of the principled MMSE denoiser. These plug-and-play denoisers typically rely on generic or hand-crafted priors, which could lead to substantial imperfection in compressive imaging applications due to oversimplification and misspecification of the prior distribution. Motivated by the above, we propose a score-based turbo message passing (STMP) algorithm that exploits the score-based models as an accurate and expressive image prior, facilitating compressive image recovery from a purely Bayesian perspective.

3 Score-Based MMSE Denoising

Theorem 1 (Tweedie’s formula and its second-order generalization). Consider $\tilde{\mathbf{x}}$ to be an AWGN observation of \mathbf{x} , i.e., $\tilde{\mathbf{x}} = \mathbf{x} + \mathbf{w}$, where the prior distribution $p(\mathbf{x})$ and the noise distribution $\mathbf{w} \sim \mathcal{N}(\mathbf{0}, \sigma^2 \mathbf{I})$ are given. The posterior mean and covariance are respectively given by

$$\mathbb{E}[\mathbf{x}|\tilde{\mathbf{x}}] = \tilde{\mathbf{x}} + \sigma^2 \nabla_{\tilde{\mathbf{x}}} \log p(\tilde{\mathbf{x}}), \quad (11)$$

$$\text{Cov}[\mathbf{x}|\tilde{\mathbf{x}}] = \sigma^2 \mathbf{I} + \sigma^4 \nabla_{\tilde{\mathbf{x}}}^2 \log p(\tilde{\mathbf{x}}). \quad (12)$$

Theorem 1 combines Tweedie’s formula [26, 11] for retrieving the posterior mean and its second-order generalization for retrieving the posterior variance [22, 12]. We provide a unified proof in Appendix A. Remarkably, Theorem 1 establishes the theoretical foundation for using score functions to achieve empirical Bayes-optimal denoising of AWGN observations. Once the score functions are known, we can apply Theorem 1 to efficiently implement the MMSE denoiser in (9) and (10). We discuss how to obtain the first- and second-order score estimates, i.e., $\nabla_{\tilde{\mathbf{x}}} \log p(\tilde{\mathbf{x}})$ and $\nabla_{\tilde{\mathbf{x}}}^2 \log p(\tilde{\mathbf{x}})$, via the denoising score matching technique [31, 29] in the following.

4 First- and Second-Order Score Matching

4.1 First-Order Score Matching

For a given σ , we aim to learn a first-order score model $\mathbf{s}_{\boldsymbol{\theta}}(\cdot, \sigma) : \mathbb{R}^N \rightarrow \mathbb{R}^N$ parameterized by $\boldsymbol{\theta}$ with the following score matching objective:

$$\min_{\boldsymbol{\theta}} \mathbb{E}_{p(\tilde{\mathbf{x}})} \left[\|\mathbf{s}_{\boldsymbol{\theta}}(\tilde{\mathbf{x}}, \sigma) - \nabla_{\tilde{\mathbf{x}}} \log p(\tilde{\mathbf{x}})\|_2^2 \right]. \quad (13)$$

The above formulation is shown equivalent to the denoising score matching objective [31, 29], given by

$$\min_{\boldsymbol{\theta}} \mathbb{E}_{p(\mathbf{x})p(\tilde{\mathbf{x}}|\mathbf{x})} \left[\|\mathbf{s}_{\boldsymbol{\theta}}(\tilde{\mathbf{x}}, \sigma) - \nabla_{\tilde{\mathbf{x}}} \log p(\tilde{\mathbf{x}}|\mathbf{x})\|_2^2 \right]. \quad (14)$$

Substituting $\nabla_{\tilde{\mathbf{x}}} \log p(\tilde{\mathbf{x}}|\mathbf{x}) = -\frac{\tilde{\mathbf{x}} - \mathbf{x}}{\sigma^2}$ into (14) yields

$$\min_{\boldsymbol{\theta}} \ell_1(\boldsymbol{\theta}; \sigma) := \mathbb{E}_{p(\mathbf{x})p(\tilde{\mathbf{x}}|\mathbf{x})} \left[\left\| \mathbf{s}_{\boldsymbol{\theta}}(\tilde{\mathbf{x}}, \sigma) + \frac{\tilde{\mathbf{x}} - \mathbf{x}}{\sigma^2} \right\|_2^2 \right]. \quad (15)$$

In practice, the score-based MMSE denoiser is required to operate effectively across a range of noise levels. We therefore combine (15) for all possible $\sigma \in \{\sigma_i\}_{i=1}^L$ to formulate the following unified objective for training the first-order score model:

$$\min_{\boldsymbol{\theta}} \mathcal{L}_1(\boldsymbol{\theta}; \{\sigma_i\}_{i=1}^L) := \frac{1}{L} \sum_{i=1}^L \lambda_1(\sigma_i) \ell_1(\boldsymbol{\theta}; \sigma_i), \quad (16)$$

where $\lambda_1(\sigma_i)$ is the weighting factor depending on σ_i .

4.2 Second-Order Score Matching

For a given σ , we aim to learn a second-order score model $\mathbf{S}_{\phi}(\cdot, \sigma) : \mathbb{R}^N \rightarrow \mathbb{R}^{N \times N}$ parameterized by ϕ with the following score matching objective:

$$\min_{\phi} \mathbb{E}_{p(\tilde{\mathbf{x}})} \left[\|\mathbf{S}_{\phi}(\tilde{\mathbf{x}}, \sigma) - \nabla_{\tilde{\mathbf{x}}}^2 \log p(\tilde{\mathbf{x}})\|_F^2 \right]. \quad (17)$$

The second-order score matching objective also has an equivalent denoising score matching formulation [19]:

$$\min_{\phi} \mathbb{E}_{p(\mathbf{x})p(\tilde{\mathbf{x}}|\mathbf{x})} \left[\left\| \mathbf{S}_{\phi}(\tilde{\mathbf{x}}, \sigma) - \mathbf{b}(\mathbf{x}, \tilde{\mathbf{x}}, \sigma) \mathbf{b}(\mathbf{x}, \tilde{\mathbf{x}}, \sigma)^{\top} + \frac{\mathbf{I}}{\sigma^2} \right\|_F^2 \right], \quad (18)$$

where $\mathbf{b}(\mathbf{x}, \tilde{\mathbf{x}}, \sigma) := \nabla_{\tilde{\mathbf{x}}} \log p(\tilde{\mathbf{x}}) + \frac{\tilde{\mathbf{x}} - \mathbf{x}}{\sigma^2}$. Please refer to Appendix B for the detailed derivation. The objective in (18) relies on the ground-truth of the first-order score function, which is in general not accessible. In practice, we replace $\nabla_{\tilde{\mathbf{x}}} \log p(\tilde{\mathbf{x}})$ by the learned $\mathbf{s}_{\boldsymbol{\theta}}(\tilde{\mathbf{x}}, \sigma)$ for efficient computation. The objective in (18) then becomes

$$\min_{\phi} \mathbb{E}_{p(\mathbf{x})p(\tilde{\mathbf{x}}|\mathbf{x})} \left[\left\| \mathbf{S}_{\phi}(\tilde{\mathbf{x}}, \sigma) - \hat{\mathbf{b}}(\mathbf{x}, \tilde{\mathbf{x}}, \sigma) \hat{\mathbf{b}}(\mathbf{x}, \tilde{\mathbf{x}}, \sigma)^{\top} + \frac{\mathbf{I}}{\sigma^2} \right\|_F^2 \right], \quad (19)$$

where $\hat{\mathbf{b}}(\mathbf{x}, \tilde{\mathbf{x}}, \sigma) := \mathbf{s}_{\boldsymbol{\theta}}(\tilde{\mathbf{x}}, \sigma) + \frac{\tilde{\mathbf{x}} - \mathbf{x}}{\sigma^2}$. It is proved in [19] that with this replacement, the second-order score model has the error-bounded property if the first-order score matching error is bounded.

As in Line 12 of Algorithm 1, only the trace of the posterior covariance matrix is needed, rather than the covariance matrix itself. By noting in (12) the simple relation between the posterior covariance matrix and the second-order score function, it suffices to only match the trace of the

Algorithm 2 STMP Algorithm

```

1: Input:  $\mathbf{A}$ ,  $\mathbf{y}$ ,  $\delta_0^2$ ,  $\mathbf{x}_A^{pri}$ ,  $v_A^{pri}$ 
2: Output:  $\mathbf{x}_B^{post}$ 
3: repeat
4:   % LMMSE estimator
5:    $\mathbf{x}_A^{post} = \mathbf{x}_A^{pri} + v_A^{pri} \mathbf{A}^\top (v_A^{pri} \mathbf{A} \mathbf{A}^\top + \delta_0^2 \mathbf{I})^{-1} (\mathbf{y} - \mathbf{A} \mathbf{x}_A^{pri})$ 
6:    $v_A^{post} = v_A^{pri} - \frac{(v_A^{pri})^2}{N} \text{tr}(\mathbf{A}^\top (v_A^{pri} \mathbf{A} \mathbf{A}^\top + \delta_0^2 \mathbf{I})^{-1} \mathbf{A})$ 
7:    $v_A^{ext} = 1 / (1/v_A^{post} - 1/v_A^{pri})$ 
8:    $\mathbf{x}_A^{ext} = v_A^{ext} (\mathbf{x}_A^{post} / v_A^{post} - \mathbf{x}_A^{pri} / v_A^{pri})$ 
9:    $\mathbf{x}_B^{pri} = \mathbf{x}_A^{ext}$ ,  $v_B^{pri} = v_A^{ext}$ 
10:  % Score-based MMSE denoiser
11:   $\mathbf{x}_B^{post} = \mathbf{x}_B^{pri} + v_B^{pri} \mathbf{s}_\theta(\mathbf{x}_B^{pri}, \sqrt{v_B^{pri}})$ 
12:   $v_B^{post} = \frac{(v_B^{pri})^2}{N} \text{tr}(\mathbf{S}_\phi(\mathbf{x}_B^{pri}, \sqrt{v_B^{pri}})) + v_B^{pri}$ 
13:   $v_B^{ext} = 1 / (1/v_B^{post} - 1/v_B^{pri})$ 
14:   $\mathbf{x}_B^{ext} = v_B^{ext} (\mathbf{x}_B^{post} / v_B^{post} - \mathbf{x}_B^{pri} / v_B^{pri})$ 
15:   $\mathbf{x}_A^{pri} = \mathbf{x}_B^{ext}$ ,  $v_A^{pri} = v_B^{ext}$ 
16: until the stopping criterion is met

```

second-order score function for posterior variance evaluation. The simplified objective is expressed as

$$\min_{\phi} \ell_2(\phi; \sigma) := \mathbb{E}_{p(\mathbf{x})p(\tilde{\mathbf{x}}|\mathbf{x})} \left[\left| \text{tr}(\mathbf{S}_\phi(\tilde{\mathbf{x}}, \sigma)) - \left\| \hat{\mathbf{b}}(\mathbf{x}, \tilde{\mathbf{x}}, \sigma) \right\|_2^2 + \frac{N}{\sigma^2} \right|^2 \right]. \quad (20)$$

We combine (20) for all $\sigma \in \{\sigma_i\}_{i=1}^L$ to obtain the following unified objective for training the second-order score model:

$$\min_{\phi} \mathcal{L}_2(\phi; \{\sigma_i\}_{i=1}^L) := \frac{1}{L} \sum_{i=1}^L \lambda_2(\sigma_i) \ell_2(\phi; \sigma_i), \quad (21)$$

where $\lambda_2(\sigma_i)$ is the weighting factor depending on σ_i . In practice, one can first train a first-order score model, and then freeze it when applied to second-order score learning. Alternatively, the two score models can be trained both at once by disabling gradient backpropagation from the second-order training objective (21) to the first-order score model.

5 STMP Algorithm

The score models, once learned, can be plugged into the Turbo-CS framework, facilitating MMSE denoising via

$$\mathbf{x}_B^{post} = \mathbf{x}_B^{pri} + v_B^{pri} \mathbf{s}_\theta(\mathbf{x}_B^{pri}, \sqrt{v_B^{pri}}), \quad (22)$$

$$v_B^{post} = \frac{(v_B^{pri})^2}{N} \text{tr}(\mathbf{S}_\phi(\mathbf{x}_B^{pri}, \sqrt{v_B^{pri}})) + v_B^{pri}. \quad (23)$$

Eqns. (22) and (23) are simply restatements of (11) and (12), respectively. Upon this replacement, we obtain the STMP algorithm in Algorithm 2. The algorithm stops when the maximum number of iterations is reached, or the difference of \mathbf{x}_B^{post} between two consecutive iterations falls below a certain threshold.

We have empirically observed that when the compression ratio M/N is low, adding damping to the message updates helps to stabilize convergence. In particular, we suggest to replace Line 9 of Algorithm 2 by

$$\mathbf{x}_B^{pri} = \beta \mathbf{x}_A^{ext} + (1 - \beta) \mathbf{x}_{A,old}^{ext}, \quad (24)$$

$$v_B^{pri} = \beta v_A^{ext} + (1 - \beta) v_{A,old}^{ext}, \quad (25)$$

where $\mathbf{x}_{A,old}^{ext}$ and $v_{A,old}^{ext}$ are the extrinsic mean and variance of module A from the last iteration, $\beta \in (0, 1]$ is the damping factor. Line 15 of Algorithm 2 should be modified similarly.

As shown in Lines 5 and 6 of Algorithm 2, the LMMSE estimator requires the computation of a different matrix inverse at each iteration with prohibitive complexity. This can be avoided by the pre-calculation of the singular value decomposition (SVD) of \mathbf{A} [25]. Moreover, in compressive imaging, the rows of \mathbf{A} are typically randomly selected from an orthogonal matrix (e.g., DCT matrix). This results in a diagonal matrix to be inverted at each iteration, which significantly reduces the computational cost.

6 State Evolution Analysis

The asymptotic MSE performance of the STMP algorithm can be accurately predicted by a set of SE equations. Due to the limited representation capability of a neural network, the score-based denoiser may not be perfectly matched with the MMSE performance at each iteration. The LMMSE estimator can also be substituted with other linear estimators, such as matched filter and pseudo-inverse [20]. Therefore, we adopt a more general notation to represent the linear estimator and the denoiser as

$$\mathbf{x}_A^{post} = \mathbf{g}_A(\mathbf{x}_A^{pri}, v_A^{pri}), \quad \mathbf{x}_B^{post} = \mathbf{g}_B(\mathbf{x}_B^{pri}, v_B^{pri}). \quad (26)$$

We make the following assumption on the posterior variances.

Assumption 1. Assume that the posterior variances perfectly match the linear estimator and the denoiser under the practical setting in (26), i.e.,

$$v_A^{post} = \frac{1}{N} \mathbb{E} \left[(\mathbf{g}_A(\mathbf{x}_A^{pri}, v_A^{pri}) - \mathbf{x})^\top (\mathbf{g}_A(\mathbf{x}_A^{pri}, v_A^{pri}) - \mathbf{x}) \right], \quad (27)$$

$$v_B^{post} = \frac{1}{N} \mathbb{E} \left[(\mathbf{g}_B(\mathbf{x}_B^{pri}, v_B^{pri}) - \mathbf{x})^\top (\mathbf{g}_B(\mathbf{x}_B^{pri}, v_B^{pri}) - \mathbf{x}) \right]. \quad (28)$$

Similar to [13], define the MSE function of the linear estimator under AWGN measurement as

$$\begin{aligned} \text{mse}_A(v_A^{pri}, \tau_A) &:= \lim_{N \rightarrow \infty} \frac{1}{N} \mathbb{E} \left[\left\| \mathbf{g}_A(\mathbf{r}_A, v_A^{pri}) - \mathbf{x} \right\|_2^2 \right], \\ \mathbf{r}_A &= \mathbf{x} + \mathcal{N}(\mathbf{0}, \tau_A \mathbf{I}), \quad \mathbf{y} = \mathbf{A} \mathbf{x} + \mathcal{N}(\mathbf{0}, \delta_0^2 \mathbf{I}), \end{aligned} \quad (29)$$

and define that of the denoiser as

$$\begin{aligned} \text{mse}_{\mathbf{B}}(v_{\mathbf{B}}^{pri}, \tau_{\mathbf{B}}) &:= \lim_{N \rightarrow \infty} \frac{1}{N} \mathbb{E} \left[\left\| \mathbf{g}_{\mathbf{B}}(\mathbf{r}_{\mathbf{B}}, v_{\mathbf{B}}^{pri}) - \mathbf{x} \right\|_2^2 \right], \\ \mathbf{r}_{\mathbf{B}} &= \mathbf{x} + \mathcal{N}(\mathbf{0}, \tau_{\mathbf{B}} \mathbf{I}). \end{aligned} \quad (30)$$

Furthermore, we define the sensitivity functions of the linear estimator and the denoiser respectively as

$$\text{sf}_{\mathbf{A}}(v_{\mathbf{A}}^{pri}, \tau_{\mathbf{A}}) := \lim_{N \rightarrow \infty} \frac{1}{N} \text{tr} \left(\frac{\partial \mathbf{g}_{\mathbf{A}}(\mathbf{r}_{\mathbf{A}}, v_{\mathbf{A}}^{pri})}{\partial \mathbf{r}_{\mathbf{A}}} \right), \quad (31)$$

$$\text{sf}_{\mathbf{B}}(v_{\mathbf{B}}^{pri}, \tau_{\mathbf{B}}) := \lim_{N \rightarrow \infty} \frac{1}{N} \text{tr} \left(\frac{\partial \mathbf{g}_{\mathbf{B}}(\mathbf{r}_{\mathbf{B}}, v_{\mathbf{B}}^{pri})}{\partial \mathbf{r}_{\mathbf{B}}} \right). \quad (32)$$

Theorem 2. Under Assumptions 1, 1, 2, and 3, the SE of the STMP algorithm at the k -th iteration is established by the following scalar equations:

$$v_{\mathbf{A},k}^{post} = v_{\mathbf{A},k}^{pri} \text{sf}_{\mathbf{A}}(v_{\mathbf{A},k}^{pri}, \tau_{\mathbf{A},k}), \quad (33)$$

$$v_{\mathbf{B},k}^{pri} = v_{\mathbf{A},k}^{ext} = \frac{v_{\mathbf{A},k}^{pri} v_{\mathbf{A},k}^{post}}{v_{\mathbf{A},k}^{pri} - v_{\mathbf{A},k}^{post}}, \quad (34)$$

$$\tau_{\mathbf{B},k} = \frac{(v_{\mathbf{A},k}^{pri})^2 \text{mse}_{\mathbf{A}}(v_{\mathbf{A},k}^{pri}, \tau_{\mathbf{A},k}) - (v_{\mathbf{A},k}^{post})^2 \tau_{\mathbf{A},k}}{(v_{\mathbf{A},k}^{pri} - v_{\mathbf{A},k}^{post})^2}, \quad (35)$$

$$v_{\mathbf{B},k}^{post} = v_{\mathbf{B},k}^{pri} \text{sf}_{\mathbf{B}}(v_{\mathbf{B},k}^{pri}, \tau_{\mathbf{B},k}), \quad (36)$$

$$v_{\mathbf{A},k+1}^{pri} = v_{\mathbf{B},k}^{ext} = \frac{v_{\mathbf{B},k}^{pri} v_{\mathbf{B},k}^{post}}{v_{\mathbf{B},k}^{pri} - v_{\mathbf{B},k}^{post}}, \quad (37)$$

$$\tau_{\mathbf{A},k+1} = \frac{(v_{\mathbf{B},k}^{pri})^2 \text{mse}_{\mathbf{B}}(v_{\mathbf{B},k}^{pri}, \tau_{\mathbf{B},k}) - (v_{\mathbf{B},k}^{post})^2 \tau_{\mathbf{B},k}}{(v_{\mathbf{B},k}^{pri} - v_{\mathbf{B},k}^{post})^2}, \quad (38)$$

in which $\tau_{\mathbf{A},k}$ and $\tau_{\mathbf{B},k}$ denote the true noise variances in the inputs of module A and module B, respectively.

Theorem 2 restates the main result presented in [13]. For the relevant assumptions, please refer to Appendix C. We initialize the equations with $\tau_{\mathbf{A},0} = v_{\mathbf{A},0}^{pri} = \mathbb{E}[\|\mathbf{x}_{\mathbf{A}}^{pri} - \mathbf{x}\|_2^2]$. At the k -th iteration, the asymptotic MSE of STMP is predicted by $\text{mse}_{\mathbf{B}}(v_{\mathbf{B},k}^{pri}, \tau_{\mathbf{B},k})$.

The SE equations can be further simplified when the score-based networks act as an MMSE denoiser. The simplified SE equations coincide with the fixed-point characterization of the Bayes-optimal MSE predicted by the replica method [25]. This implies that STMP can potentially achieve the Bayes-optimal MSE performance with a perfectly learned MMSE denoiser.

7 Experiments

In this section, we evaluate the performance of the proposed method based on the FFHQ 256×256 dataset [16].

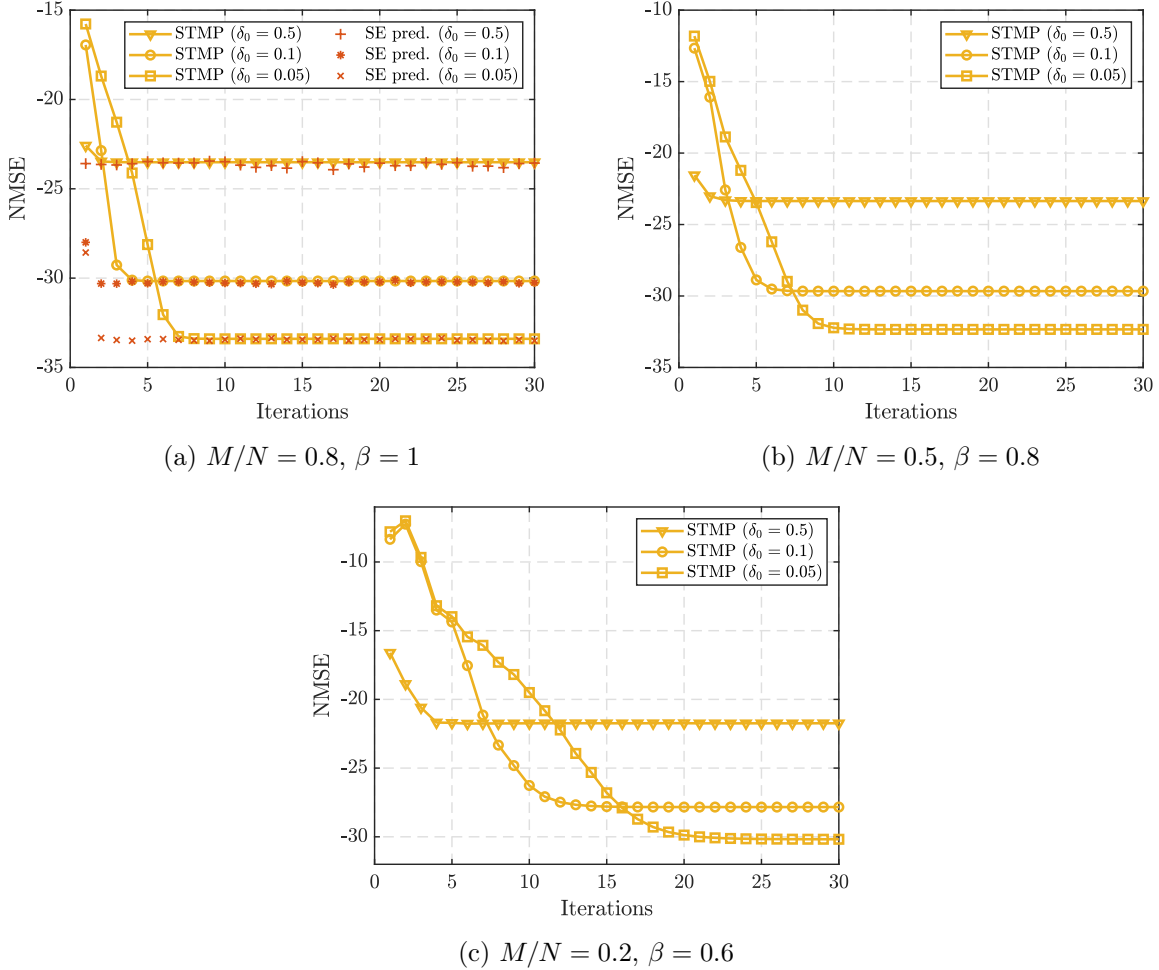


Figure 3: Convergence behaviors (one experiment) of STMP for different compression ratios and noise levels.

Training and inference configurations. We adopt the pre-trained score function in [30] as our first-order score model. Unfortunately, there is no publicly available second-order score model on the FFHQ dataset. For training the second-order score model, we adopt the NCSN++ architecture [30] that outputs only the diagonal value of the second-order score, yielding the same output dimension as the first-order score model. The focus on the diagonal is due to the fact that only the trace of the second-order score is pertinent to the calculation of the loss function in (21). The first-order score model is adopted to provide the corresponding estimate in (21). The training of the second-order score model follows the same default settings as its first-order counterpart [30]; see Appendix D.1 for more details. For inference, we test our proposed method and several benchmarks on 1000 images from the validation set of the FFHQ dataset.

Task specification. We consider a compressive image recovery task with the measurement matrix in the form of $\mathbf{A} = \mathbf{S}\mathbf{W}\mathbf{\Theta}$, where $\mathbf{S} \in \mathbb{R}^{M \times N}$ is a random row selection matrix consisting of randomly selected rows from a permutation matrix, $\mathbf{W} \in \mathbb{R}^{N \times N}$ is a DCT matrix, and $\mathbf{\Theta} \in \mathbb{R}^{N \times N}$ is a diagonal

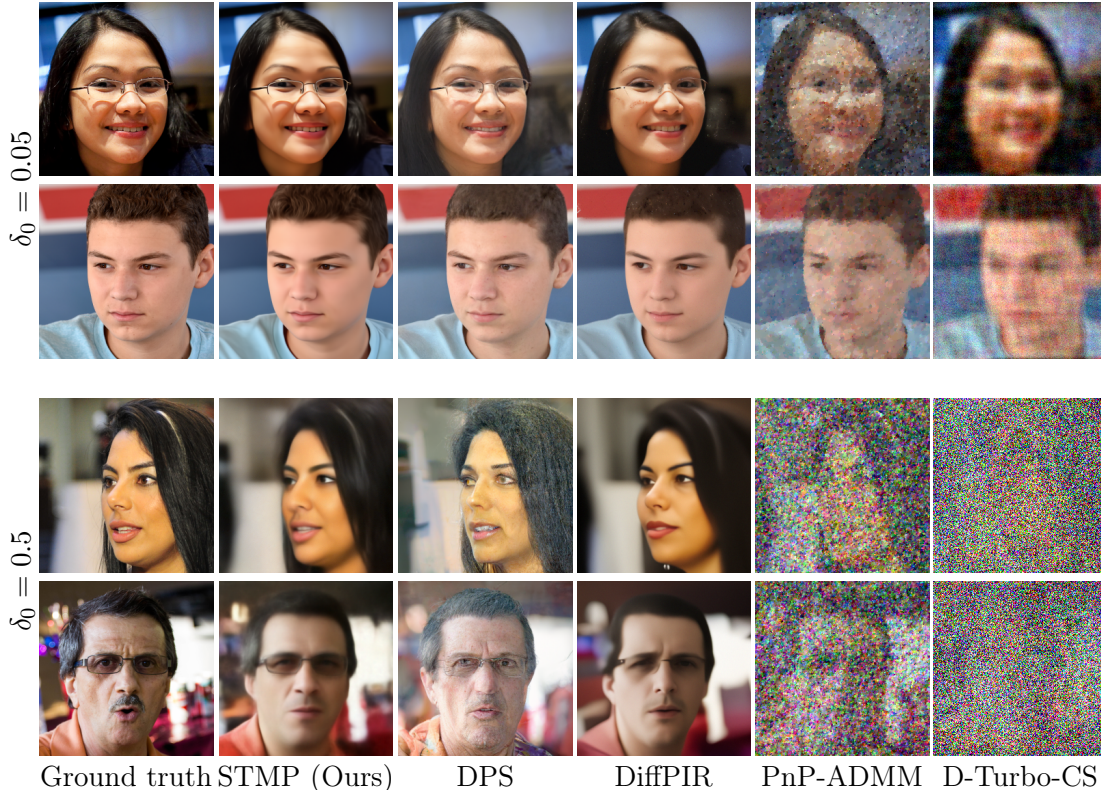


Figure 4: Representative results on FFHQ validation set. The compression ratio is $M/N = 0.1$ and we set $\beta = 0.5$.

matrix with random signs (1 or -1) in the diagonal. We provide comprehensive results on the image recovery performance under different compression ratios and noise levels.

Benchmarks. We compare our proposed method against both the recent state-of-the-art score-based posterior sampling techniques and the traditional plug-and-play methods. The baselines include diffusion posterior sampling (DPS) [6], diffusion models for plug-and-play image restoration (DiffPIR) [36], plug-and-play alternating direction method of multipliers (PnP-ADMM) [4], and denoising-based turbo compressed sensing (D-Turbo-CS) [34]. As suggested in [6, 36], we set the number reverse timesteps (i.e., NFEs) in DPS and DiffPIR as 1000 and 100, respectively. We choose the total variation (TV) denoising method as the plug-and-play denoiser in PnP-ADMM, and choose the SURE-LET [3] denoiser for D-Turbo-CS. We provide in Appendix D.2 the hyperparameters used in these benchmarks.

Convergence behaviors and state evolution. Fig. 3 reports the normalized MSE (NMSE) of the reconstruction during the execution of STMP. Overall, the proposed algorithm exhibits a fast convergence speed under different compression ratios M/N and noise levels δ_0 . The number of iterations required to reach convergence increases as the ratio M/N decreases, since recovering from fewer observations is more ill-posed and challenging. Moreover, the proposed algorithm converges slightly slower with a small added noise. It recovers more details of the ground-truth image from

Table 1: Quantitative results on FFHQ validation set. The compression ratio is $M/N = 0.1$ and we set $\beta = 0.5$.

Method	$\delta_0 = 0.5$				$\delta_0 = 0.05$			
	PSNR \uparrow	SSIM \uparrow	FID \downarrow	LPIPS \downarrow	PSNR \uparrow	SSIM \uparrow	FID \downarrow	LPIPS \downarrow
STMP (Ours)	22.07	0.6447	<u>68.85</u>	0.0640	29.86	0.8615	<u>46.09</u>	0.0146
DPS	14.01	0.4447	56.23	0.1430	22.15	0.7170	29.36	0.0287
DiffPIR	<u>21.07</u>	<u>0.6149</u>	97.38	<u>0.0765</u>	<u>25.52</u>	<u>0.7539</u>	56.30	<u>0.0270</u>
PnP-ADMM	11.46	0.0638	374.52	0.4526	19.16	0.4646	310.09	0.0827
D-Turbo-CS	5.77	0.0045	427.89	0.9031	19.15	0.2072	251.94	0.1558

relatively “clean” observations.

We present the SE prediction only in Fig. 3(a) because the adoption of damping in the other two subfigures makes the SE inaccurate. Overall, the SE equations accurately predict the converged performance of STMP. It is also observed that, before convergence, there is a mismatch between the SE prediction and the actual performance of STMP. We conjecture that this discrepancy stems from the training errors in second-order denoising score matching, leading to a deviation of the estimated posterior variance from Assumption 1.

Qualitative results. We present some representative results in Fig. 4. Both PnP-ADMM and D-Turbo-CS fail to produce satisfactory results due to the extremely low compression ratio ($M/N = 0.1$). When the added noise is small ($\delta_0 = 0.05$), the proposed method, DPS, and DiffPIR are able to generate high-quality reconstructions. The DPS baseline, however, does not always adhere to the ground-truth image when the added noise is large ($\delta_0 = 0.5$). For example, in the last row of Fig. 4, the sample generated by DPS depicts a man wearing transparent glasses, whereas the ground truth shows sunglasses. This highlights the superior restoration fidelity of our method over DPS. More results on different compression ratios and noise levels can be found in Appendix E.

Quantitative results. In Table 1, we report the average peak signal-to-noise ratio (PSNR), structural similarity index measure (SSIM) [33], Fréchet inception distance (FID) [14], and learned perceptual image patch similarity (LPIPS) [35] to evaluate the faithfulness to the original image and the visual quality. We see that our proposed algorithm outperforms other benchmarks on most of these metrics. More results can be found in Appendix E.

Performance-complexity tradeoff. The computational complexity of STMP, DPS, and DiffPIR is dominated by the number of NFEs. In STMP, each iteration involves forward propagation through both the first- and the second-order score networks. Although these two NFEs can be executed in parallel without doubling the time consumption, we still regard each iteration as involving two NFEs. We evaluate the tradeoff between the reconstruction faithfulness/image quality and the computational complexity in Fig. 5. Compared to the other two benchmarks, STMP requires

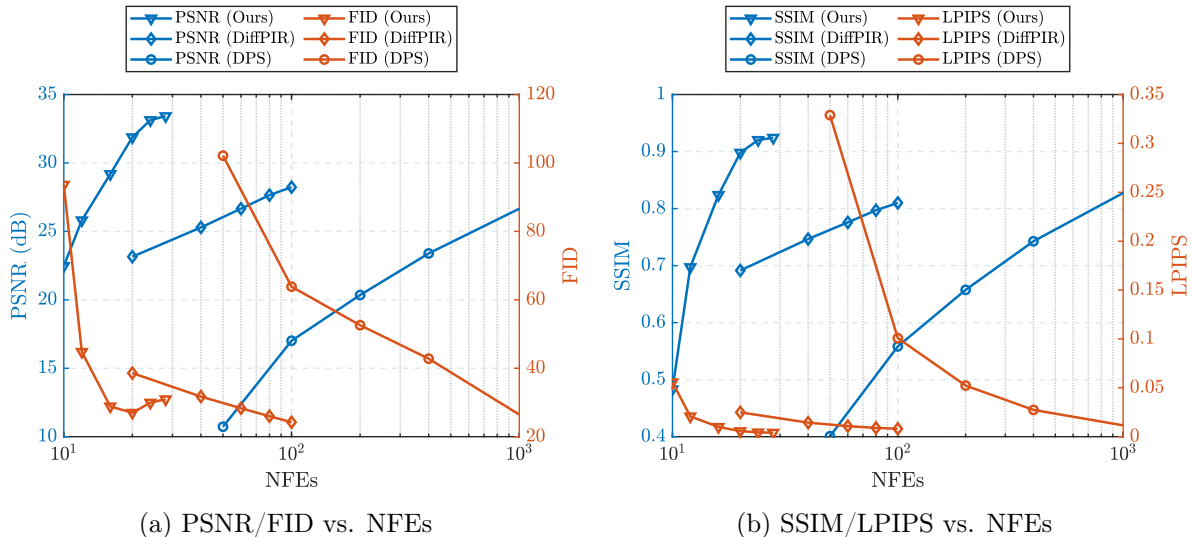


Figure 5: Tradeoff between the reconstruction faithfulness/image quality and the computational complexity. The compression ratio is $M/N = 0.4$ and the noise level is $\delta_0 = 0.05$. We set $\beta = 0.8$.

significantly fewer NFEs to produce meaningful results, highlighting the efficiency of our design. Note that DPS requires not only forward propagation during each NFE, but also back-propagating gradients through the score-based network. This makes the sampling steps in DPS even more computationally expensive.

8 Conclusion

In this paper, we introduced score-based turbo message passing (STMP), a novel approach for compressive image recovery using unconditional score-based networks. STMP inherits the fast convergence speed of message passing algorithms and, meanwhile, takes full advantage of the expressive prior through the integration of score-based networks. Theoretically, we demonstrated that the asymptotic performance of STMP can be predicted by a set of scalar equations called state evolution (SE). Experimental results on the FFHQ dataset showcase the state-of-the-art performance of STMP against different benchmarks. This paper lays the groundwork for further enhancing the efficiency of linear inverse problem solving. By making straightforward adjustments to the message calculation in the linear estimation part, STMP can be generalized to address a broader class of inverse problems.

References

- [1] C. Berrou and A. Glavieux. Near optimum error correcting coding and decoding: Turbo-codes. *IEEE Transactions on Communications*, 44(10):1261–1271, 1996. doi: 10.1109/26.539767.
- [2] C. M. Bishop. *Pattern Recognition and Machine Learning*. Springer, Berlin, Germany, 2006.

- [3] T. Blu and F. Luisier. The SURE-LET approach to image denoising. *IEEE Transactions on Image Processing*, 16(11):2778–2786, 2007.
- [4] S. H. Chan, X. Wang, and O. A. Elgandy. Plug-and-play ADMM for image restoration: Fixed-point convergence and applications. *IEEE Transactions on Computational Imaging*, 3(1):84–98, 2017.
- [5] H. Chung, B. Sim, D. Ryu, and J. C. Ye. Improving diffusion models for inverse problems using manifold constraints. In *Proceedings of the Advances in Neural Information Processing Systems*, 2022.
- [6] H. Chung, J. Kim, M. T. McCann, M. L. Klasky, and J. C. Ye. Diffusion posterior sampling for general noisy inverse problems. In *Proceedings of the International Conference on Learning Representations*, 2023.
- [7] K. Dabov, A. Foi, V. Katkovnik, and K. Egiazarian. Image denoising with block-matching and 3D filtering. In *Image processing: algorithms and systems, neural networks, and machine learning*, volume 6064, pages 354–365. SPIE, 2006.
- [8] G. Daras, H. Chung, C.-H. Lai, Y. Mitsufuji, J. C. Ye, P. Milanfar, A. G. Dimakis, and M. Delbracio. A survey on diffusion models for inverse problems. <https://arxiv.org/abs/2410.00083>, 2024.
- [9] D. L. Donoho, A. Maleki, and A. Montanari. Message-passing algorithms for compressed sensing. *Proceedings of the National Academy of Sciences*, 106(45):18914–18919, 2009.
- [10] Z. Dou and Y. Song. Diffusion posterior sampling for linear inverse problem solving: A filtering perspective. In *Proceedings of the International Conference on Learning Representations*, 2024.
- [11] B. Efron. Tweedie’s formula and selection bias. *Journal of the American Statistical Association*, 106(496):1602–1614, 2011.
- [12] M. A. Finzi, A. Boral, A. G. Wilson, F. Sha, and L. Zepeda-Núñez. User-defined event sampling and uncertainty quantification in diffusion models for physical dynamical systems. In *Proceedings of the International Conference on Machine Learning*, pages 10136–10152. PMLR, 2023.
- [13] A. K. Fletcher, P. Pandit, S. Rangan, S. Sarkar, and P. Schniter. Plug-in estimation in high-dimensional linear inverse problems: A rigorous analysis. In *Proceedings of the Advances in Neural Information Processing Systems*, pages 7451–7460, 2018.
- [14] M. Heusel, H. Ramsauer, T. Unterthiner, B. Nessler, and S. Hochreiter. GANs trained by a two time-scale update rule converge to a local nash equilibrium. In *Proceedings of the Advances in Neural Information Processing Systems*, pages 6626–6637, 2017.

- [15] J. Ho, A. Jain, and P. Abbeel. Denoising diffusion probabilistic models. In *Proceedings of the Advances in Neural Information Processing Systems*, volume 33, pages 6840–6851, 2020.
- [16] T. Karras, S. Laine, and T. Aila. A style-based generator architecture for generative adversarial networks. In *Proceedings of the IEEE/CVF Conference on Computer Vision and Pattern Recognition*, pages 4401–4410. IEEE, 2019.
- [17] B. Kawar, G. Vaksman, and M. Elad. SNIPS: Solving noisy inverse problems stochastically. In *Proceedings of the Advances in Neural Information Processing Systems*, volume 34, pages 21757–21769, 2021.
- [18] B. Kawar, M. Elad, S. Ermon, and J. Song. Denoising diffusion restoration models. In *Proceedings of the Advances in Neural Information Processing Systems*, volume 35, pages 23593–23606, 2022.
- [19] C. Lu, K. Zheng, F. Bao, J. Chen, C. Li, and J. Zhu. Maximum likelihood training for score-based diffusion odes by high order denoising score matching. In *Proceedings of the International Conference on Machine Learning*, pages 14429–14460. PMLR, 2022.
- [20] J. Ma and L. Ping. Orthogonal AMP. *IEEE Access*, 5:2020–2033, 2017.
- [21] J. Ma, X. Yuan, and L. Ping. Turbo compressed sensing with partial DFT sensing matrix. *IEEE Signal Processing Letters*, 22(2):158–161, 2015.
- [22] C. Meng, Y. Song, W. Li, and S. Ermon. Estimating high order gradients of the data distribution by denoising. In *Proceedings of the Advances in Neural Information Processing Systems*, volume 34, pages 25359–25369, 2021.
- [23] C. Metzler, A. Mousavi, and R. Baraniuk. Learned D-AMP: Principled neural network based compressive image recovery. In *Proceedings of the Advances in Neural Information Processing Systems*, volume 30, 2017.
- [24] C. A. Metzler, A. Maleki, and R. G. Baraniuk. From denoising to compressed sensing. *IEEE Transactions on Information Theory*, 62(9):5117–5144, 2016.
- [25] S. Rangan, P. Schniter, and A. K. Fletcher. Vector approximate message passing. *IEEE Transactions on Information Theory*, 65(10):6664–6684, 2019.
- [26] H. E. Robbins. An empirical bayes approach to statistics. In *Breakthroughs in Statistics: Foundations and basic theory*, pages 388–394. Springer, 1992.
- [27] P. Schniter, S. Rangan, and A. Fletcher. Denoising based vector approximate message passing. <https://arxiv.org/abs/1611.01376>, 2016.
- [28] J. Song, A. Vahdat, M. Mardani, and J. Kautz. Pseudoinverse-guided diffusion models for inverse problems. In *Proceedings of the International Conference on Learning Representations*, 2023.

- [29] Y. Song and S. Ermon. Generative modeling by estimating gradients of the data distribution. In *Proceedings of the Advances in Neural Information Processing Systems*, volume 32, 2019.
- [30] Y. Song, J. Sohl-Dickstein, D. P. Kingma, A. Kumar, S. Ermon, and B. Poole. Score-based generative modeling through stochastic differential equations. In *Proceedings of the International Conference on Learning Representations*, 2021.
- [31] P. Vincent. A connection between score matching and denoising autoencoders. *Neural Comput.*, 23(7):1661–1674, 2011.
- [32] H. Wang, Z. Li, and X. Hou. Versatile denoising-based approximate message passing for compressive sensing. *IEEE Transactions on Image Processing*, 32:2761–2775, 2023.
- [33] Z. Wang, A. Bovik, H. Sheikh, and E. Simoncelli. Image quality assessment: from error visibility to structural similarity. *IEEE Transactions on Image Processing*, 13(4):600–612, 2004.
- [34] Z. Xue, J. Ma, and X. Yuan. Denoising-based turbo compressed sensing. *IEEE Access*, 5: 7193–7204, 2017. doi: 10.1109/ACCESS.2017.2697978.
- [35] R. Zhang, P. Isola, A. A. Efros, E. Shechtman, and O. Wang. The unreasonable effectiveness of deep features as a perceptual metric. In *Proceedings of the IEEE/CVF Conference on Computer Vision and Pattern Recognition*, pages 586–595, 2018.
- [36] Y. Zhu, K. Zhang, J. Liang, J. Cao, B. Wen, R. Timofte, and L. V. Gool. Denoising diffusion models for plug-and-play image restoration. In *IEEE/CVF Conference on Computer Vision and Pattern Recognition, CVPR 2023 Workshops*, pages 1219–1229. IEEE, 2023.
- [37] Q. Zou and H. Yang. A concise tutorial on approximate message passing. <https://arxiv.org/abs/2201.07487>, 2022.

Appendix

A Proof of Theorem 1

We express the likelihood $p(\tilde{\mathbf{x}}|\mathbf{x})$ in exponential family form as

$$p(\tilde{\mathbf{x}}|\mathbf{x}) = h(\tilde{\mathbf{x}}) \exp \left\{ \mathbf{x}^\top \boldsymbol{\varphi}(\tilde{\mathbf{x}}) - A(\mathbf{x}) \right\}, \quad (39)$$

where $h(\tilde{\mathbf{x}}) := (2\pi\sigma^2)^{-\frac{N}{2}} \exp \left\{ -\frac{\tilde{\mathbf{x}}^\top \tilde{\mathbf{x}}}{2\sigma^2} \right\}$ is the base measure, $\boldsymbol{\varphi}(\tilde{\mathbf{x}}) := \frac{\tilde{\mathbf{x}}}{\sigma^2}$ is the sufficient statistic, and $A(\mathbf{x}) := \frac{\mathbf{x}^\top \mathbf{x}}{2\sigma^2}$ is the cumulant function (a.k.a. log-partition function). Eqn. (39) corresponds to the exponential family form of the Gaussian distribution with unknown mean \mathbf{x} and known covariance matrix $\sigma^2 \mathbf{I}$. Note that since the covariance matrix is assumed known, the sufficient statistic $\boldsymbol{\varphi}(\tilde{\mathbf{x}})$ incorporates only the first-order component of $\tilde{\mathbf{x}}$.

By applying the Bayes rule, we can also write the posterior distribution in exponential family form as

$$p(\mathbf{x}|\tilde{\mathbf{x}}) = \frac{p(\mathbf{x})h(\tilde{\mathbf{x}}) \exp \left\{ \mathbf{x}^\top \boldsymbol{\varphi}(\tilde{\mathbf{x}}) - A(\mathbf{x}) \right\}}{p(\tilde{\mathbf{x}})} \quad (40)$$

$$= \bar{h}(\mathbf{x}) \exp \left\{ \tilde{\mathbf{x}}^\top \bar{\boldsymbol{\varphi}}(\mathbf{x}) - \bar{A}(\tilde{\mathbf{x}}) \right\}, \quad (41)$$

where $\bar{h}(\mathbf{x}) := p(\mathbf{x}) \exp \{-A(\mathbf{x})\}$, $\bar{\boldsymbol{\varphi}}(\mathbf{x}) := \frac{\mathbf{x}}{\sigma^2}$, and $\bar{A}(\tilde{\mathbf{x}}) := \log \frac{p(\tilde{\mathbf{x}})}{h(\tilde{\mathbf{x}})}$.

For exponential families, the mean and covariance matrix of the sufficient statistics can be calculated by taking the first- and second-order derivatives of the cumulant function, respectively [2]. That is,

$$\mathbb{E} [\bar{\boldsymbol{\varphi}}(\mathbf{x})|\tilde{\mathbf{x}}] = \nabla_{\tilde{\mathbf{x}}} \bar{A}(\tilde{\mathbf{x}}) = \nabla_{\tilde{\mathbf{x}}} \log p(\tilde{\mathbf{x}}) - \nabla_{\tilde{\mathbf{x}}} \log h(\tilde{\mathbf{x}}), \quad (42)$$

$$\text{Cov} [\bar{\boldsymbol{\varphi}}(\mathbf{x})|\tilde{\mathbf{x}}] = \nabla_{\tilde{\mathbf{x}}}^2 \bar{A}(\tilde{\mathbf{x}}) = \nabla_{\tilde{\mathbf{x}}}^2 \log p(\tilde{\mathbf{x}}) - \nabla_{\tilde{\mathbf{x}}}^2 \log h(\tilde{\mathbf{x}}). \quad (43)$$

Similar relationships hold for higher-order moments of the sufficient statistics. Substituting $\bar{\boldsymbol{\varphi}}(\mathbf{x}) = \frac{\mathbf{x}}{\sigma^2}$ and $h(\tilde{\mathbf{x}}) = (2\pi\sigma^2)^{-\frac{N}{2}} \exp \left\{ -\frac{\tilde{\mathbf{x}}^\top \tilde{\mathbf{x}}}{2\sigma^2} \right\}$ into (42) and (43) yields the desired result in Theorem 1.

B Derivation of the Second-Order Denoising Score Matching

We provide in Lemma 1 an expectation formulation of the first-order score function.

Lemma 1. *For $(\mathbf{x}, \tilde{\mathbf{x}}) \sim p(\mathbf{x}, \tilde{\mathbf{x}})$, we have*

$$\nabla_{\tilde{\mathbf{x}}} \log p(\tilde{\mathbf{x}}) = \mathbb{E}_{p(\mathbf{x}|\tilde{\mathbf{x}})} [\nabla_{\tilde{\mathbf{x}}} \log p(\tilde{\mathbf{x}}|\mathbf{x})]. \quad (44)$$

Proof.

$$\nabla_{\tilde{\mathbf{x}}} \log p(\tilde{\mathbf{x}}) = \frac{\nabla_{\tilde{\mathbf{x}}} p(\tilde{\mathbf{x}})}{p(\tilde{\mathbf{x}})} \quad (45)$$

$$= \frac{\nabla_{\tilde{\mathbf{x}}} \int p(\mathbf{x}) p(\tilde{\mathbf{x}}|\mathbf{x}) d\mathbf{x}}{p(\tilde{\mathbf{x}})} \quad (46)$$

$$= \int \frac{p(\mathbf{x}) p(\tilde{\mathbf{x}}|\mathbf{x})}{p(\tilde{\mathbf{x}})} \frac{\nabla_{\tilde{\mathbf{x}}} p(\tilde{\mathbf{x}}|\mathbf{x})}{p(\tilde{\mathbf{x}}|\mathbf{x})} d\mathbf{x} \quad (47)$$

$$= \int p(\mathbf{x}|\tilde{\mathbf{x}}) \nabla_{\tilde{\mathbf{x}}} \log p(\tilde{\mathbf{x}}|\mathbf{x}) d\mathbf{x} \quad (48)$$

$$= \mathbb{E}_{p(\mathbf{x}|\tilde{\mathbf{x}})} [\nabla_{\tilde{\mathbf{x}}} \log p(\tilde{\mathbf{x}}|\mathbf{x})]. \quad (49)$$

□

We provide in Lemma 2 an expectation formulation of the second-order score function.

Lemma 2. For $(\mathbf{x}, \tilde{\mathbf{x}}) \sim p(\mathbf{x}, \tilde{\mathbf{x}})$, we have

$$\nabla_{\tilde{\mathbf{x}}}^2 \log p(\tilde{\mathbf{x}}) = \mathbb{E}_{p(\mathbf{x}|\tilde{\mathbf{x}})} \left[\nabla_{\tilde{\mathbf{x}}}^2 \log p(\tilde{\mathbf{x}}|\mathbf{x}) + \mathbf{b}(\mathbf{x}, \tilde{\mathbf{x}}) \mathbf{b}(\mathbf{x}, \tilde{\mathbf{x}})^\top \right], \quad (50)$$

where $\mathbf{b}(\mathbf{x}, \tilde{\mathbf{x}}) := \nabla_{\tilde{\mathbf{x}}} \log p(\tilde{\mathbf{x}}) - \nabla_{\tilde{\mathbf{x}}} \log p(\tilde{\mathbf{x}}|\mathbf{x})$.

Proof. Firstly, the gradient of $p(\mathbf{x}|\tilde{\mathbf{x}})$ w.r.t. $\tilde{\mathbf{x}}$ can be calculated as

$$\nabla_{\tilde{\mathbf{x}}} p(\mathbf{x}|\tilde{\mathbf{x}}) = \nabla_{\tilde{\mathbf{x}}} \frac{p(\mathbf{x}) p(\tilde{\mathbf{x}}|\mathbf{x})}{p(\tilde{\mathbf{x}})} \quad (51)$$

$$= p(\mathbf{x}) \frac{p(\tilde{\mathbf{x}}) \nabla_{\tilde{\mathbf{x}}} p(\tilde{\mathbf{x}}|\mathbf{x}) - p(\tilde{\mathbf{x}}|\mathbf{x}) \nabla_{\tilde{\mathbf{x}}} p(\tilde{\mathbf{x}})}{p(\tilde{\mathbf{x}})^2} \quad (52)$$

$$= \frac{p(\mathbf{x}) p(\tilde{\mathbf{x}}|\mathbf{x})}{p(\tilde{\mathbf{x}})} \left(\frac{\nabla_{\tilde{\mathbf{x}}} p(\tilde{\mathbf{x}}|\mathbf{x})}{p(\tilde{\mathbf{x}}|\mathbf{x})} - \frac{\nabla_{\tilde{\mathbf{x}}} p(\tilde{\mathbf{x}})}{p(\tilde{\mathbf{x}})} \right) \quad (53)$$

$$= p(\mathbf{x}|\tilde{\mathbf{x}}) (\nabla_{\tilde{\mathbf{x}}} \log p(\tilde{\mathbf{x}}|\mathbf{x}) - \nabla_{\tilde{\mathbf{x}}} \log p(\tilde{\mathbf{x}})). \quad (54)$$

Then, we apply Lemma 1 to the second-order score function:

$$\nabla_{\tilde{\mathbf{x}}}^2 \log p(\tilde{\mathbf{x}}) = \nabla_{\tilde{\mathbf{x}}} \mathbb{E}_{p(\mathbf{x}|\tilde{\mathbf{x}})} [\nabla_{\tilde{\mathbf{x}}} \log p(\tilde{\mathbf{x}}|\mathbf{x})] \quad (55)$$

$$= \int \left(p(\mathbf{x}|\tilde{\mathbf{x}}) \nabla_{\tilde{\mathbf{x}}}^2 \log p(\tilde{\mathbf{x}}|\mathbf{x}) + \nabla_{\tilde{\mathbf{x}}} p(\mathbf{x}|\tilde{\mathbf{x}}) \nabla_{\tilde{\mathbf{x}}} \log p(\tilde{\mathbf{x}}|\mathbf{x})^\top \right) d\mathbf{x} \quad (56)$$

$$= \mathbb{E}_{p(\mathbf{x}|\tilde{\mathbf{x}})} \left[\nabla_{\tilde{\mathbf{x}}}^2 \log p(\tilde{\mathbf{x}}|\mathbf{x}) + (\nabla_{\tilde{\mathbf{x}}} \log p(\tilde{\mathbf{x}}|\mathbf{x}) - \nabla_{\tilde{\mathbf{x}}} \log p(\tilde{\mathbf{x}})) \nabla_{\tilde{\mathbf{x}}} \log p(\tilde{\mathbf{x}}|\mathbf{x})^\top \right], \quad (57)$$

$$= \mathbb{E}_{p(\mathbf{x}|\tilde{\mathbf{x}})} \left[\nabla_{\tilde{\mathbf{x}}}^2 \log p(\tilde{\mathbf{x}}|\mathbf{x}) - \mathbf{b}(\mathbf{x}, \tilde{\mathbf{x}}) \nabla_{\tilde{\mathbf{x}}} \log p(\tilde{\mathbf{x}}|\mathbf{x})^\top \right], \quad (58)$$

where (57) applies the result in (54). From Lemma 1, we also have

$$\mathbb{E}_{p(\mathbf{x}|\tilde{\mathbf{x}})} [\mathbf{b}(\mathbf{x}, \tilde{\mathbf{x}})] = \mathbb{E}_{p(\mathbf{x}|\tilde{\mathbf{x}})} [\nabla_{\tilde{\mathbf{x}}} \log p(\tilde{\mathbf{x}}) - \nabla_{\tilde{\mathbf{x}}} \log p(\tilde{\mathbf{x}}|\mathbf{x})] \quad (59)$$

$$= \nabla_{\tilde{\mathbf{x}}} \log p(\tilde{\mathbf{x}}) - \mathbb{E}_{p(\mathbf{x}|\tilde{\mathbf{x}})} [\nabla_{\tilde{\mathbf{x}}} \log p(\tilde{\mathbf{x}}|\mathbf{x})] \quad (60)$$

$$= \mathbf{0}, \quad (61)$$

and therefore

$$\mathbb{E}_{p(\mathbf{x}|\tilde{\mathbf{x}})} \left[\mathbf{b}(\mathbf{x}, \tilde{\mathbf{x}}) \nabla_{\tilde{\mathbf{x}}} \log p(\tilde{\mathbf{x}})^\top \right] = \mathbb{E}_{p(\mathbf{x}|\tilde{\mathbf{x}})} [\mathbf{b}(\mathbf{x}, \tilde{\mathbf{x}})] \nabla_{\tilde{\mathbf{x}}} \log p(\tilde{\mathbf{x}})^\top = \mathbf{0}. \quad (62)$$

Thus, we can further transform (58) by adding $\mathbf{0}$ as

$$\nabla_{\tilde{\mathbf{x}}}^2 \log p(\tilde{\mathbf{x}}) = \mathbb{E}_{p(\mathbf{x}|\tilde{\mathbf{x}})} \left[\nabla_{\tilde{\mathbf{x}}}^2 \log p(\tilde{\mathbf{x}}|\mathbf{x}) - \mathbf{b}(\mathbf{x}, \tilde{\mathbf{x}}) \nabla_{\tilde{\mathbf{x}}} \log p(\tilde{\mathbf{x}}|\mathbf{x})^\top \right] + \mathbb{E}_{p(\mathbf{x}|\tilde{\mathbf{x}})} \left[\mathbf{b}(\mathbf{x}, \tilde{\mathbf{x}}) \nabla_{\tilde{\mathbf{x}}} \log p(\tilde{\mathbf{x}})^\top \right] \quad (63)$$

$$= \mathbb{E}_{p(\mathbf{x}|\tilde{\mathbf{x}})} \left[\nabla_{\tilde{\mathbf{x}}}^2 \log p(\tilde{\mathbf{x}}|\mathbf{x}) + \mathbf{b}(\mathbf{x}, \tilde{\mathbf{x}}) \mathbf{b}(\mathbf{x}, \tilde{\mathbf{x}})^\top \right], \quad (64)$$

which completes the proof of Lemma 2. \square

By noting that $\nabla_{\tilde{\mathbf{x}}} \log p(\tilde{\mathbf{x}}|\mathbf{x}) = -\frac{\tilde{\mathbf{x}}-\mathbf{x}}{\sigma^2}$ and $\nabla_{\tilde{\mathbf{x}}}^2 \log p(\tilde{\mathbf{x}}|\mathbf{x}) = -\frac{\mathbf{I}}{\sigma^2}$, we rewrite (18) as

$$\min_{\phi} \mathbb{E}_{p(\tilde{\mathbf{x}})} \mathbb{E}_{p(\mathbf{x}|\tilde{\mathbf{x}})} \left[\left\| \mathbf{S}_{\phi}(\tilde{\mathbf{x}}, \sigma) - \mathbf{b}(\mathbf{x}, \tilde{\mathbf{x}}, \sigma) \mathbf{b}(\mathbf{x}, \tilde{\mathbf{x}}, \sigma)^\top - \nabla_{\tilde{\mathbf{x}}}^2 \log p(\tilde{\mathbf{x}}|\mathbf{x}) \right\|_F^2 \right]. \quad (65)$$

Note that the dependence on σ in $\mathbf{b}(\mathbf{x}, \tilde{\mathbf{x}}, \sigma)$ is sometimes omitted to simplify the notation. In (65), minimizing the inner expectation is an MMSE problem, whose optimal solution satisfies

$$\mathbf{S}_{\phi^*}(\tilde{\mathbf{x}}, \sigma) = \mathbb{E}_{p(\mathbf{x}|\tilde{\mathbf{x}})} \left[\mathbf{b}(\mathbf{x}, \tilde{\mathbf{x}}, \sigma) \mathbf{b}(\mathbf{x}, \tilde{\mathbf{x}}, \sigma)^\top + \nabla_{\tilde{\mathbf{x}}}^2 \log p(\tilde{\mathbf{x}}|\mathbf{x}) \right]. \quad (66)$$

Applying Lemma 2 to (66) yields

$$\mathbf{S}_{\phi^*}(\tilde{\mathbf{x}}, \sigma) = \nabla_{\tilde{\mathbf{x}}}^2 \log p(\tilde{\mathbf{x}}), \quad (67)$$

which completes the proof.

C Supplementary Information for State Evolution Analysis

C.1 Additional Assumptions

Assumption 1 (Right rotationally invariant). The distribution of \mathbf{A} is equal to that of $\mathbf{A}\mathbf{V}$ for any orthogonal matrix \mathbf{V} , independent of \mathbf{A} .

Assumption 2 (Uniformly Lipschitz continuous). The denoiser $\mathbf{g}_{\mathbf{B}}(\cdot)$ is uniformly Lipschitz continuous with parameters $\alpha_1, \alpha_2, \alpha_3$, i.e.,

$$\|\mathbf{g}_{\mathbf{B}}(\mathbf{r}_2, v_2) - \mathbf{g}_{\mathbf{B}}(\mathbf{r}_1, v_1)\| \leq (\alpha_1 + \alpha_2|v_2 - v_1|) \|\mathbf{r}_2 - \mathbf{r}_1\| + \alpha_3 \sqrt{N} |v_2 - v_1|, \quad (68)$$

for any $\mathbf{r}_1, \mathbf{r}_2, v_1, v_2$, and N .

Assumption 3 (Convergent under Gaussian noise). The vector $\mathbf{x} \in \mathbb{R}^N$ and the denoiser $\mathbf{g}_{\mathbf{B}}(\cdot)$ are convergent under Gaussian noise. Specifically, let $\mathbf{w}_1, \mathbf{w}_2 \in \mathbb{R}^N$ be two vectors where (w_{1n}, w_{2n}) are i.i.d. with $(w_{1n}, w_{2n}) = \mathcal{N}(\mathbf{0}, \mathbf{S})$ for some positive definite covariance $\mathbf{S} \in \mathbb{R}^{2 \times 2}$. The following limits exist almost surely:

$$\lim_{N \rightarrow \infty} \frac{1}{N} \mathbf{g}_{\mathbf{B}}(\mathbf{x} + \mathbf{w}_1, v_1)^\top \mathbf{g}_{\mathbf{B}}(\mathbf{x} + \mathbf{w}_2, v_2), \quad \lim_{N \rightarrow \infty} \frac{1}{N} \mathbf{g}_{\mathbf{B}}(\mathbf{x} + \mathbf{z}_1, v_1)^\top \mathbf{x}, \quad (69)$$

$$\lim_{N \rightarrow \infty} \frac{1}{N} \mathbf{x}^\top \mathbf{w}_1, \quad \lim_{N \rightarrow \infty} \frac{1}{N} \|\mathbf{x}\|_2^2, \quad (70)$$

$$\lim_{N \rightarrow \infty} \frac{1}{N} \mathbf{g}(\mathbf{x} + \mathbf{w}_1, v_1)^\top \mathbf{w}_2, \quad (71)$$

Table 2: One-to-one correspondence between the SE variables in this paper and these in [13].

Variable in [13]	Variable in this paper	Variable in [13]	Variable in this paper
$\bar{\alpha}_{1k}$	$v_{\mathbf{B},k}^{post}/v_{\mathbf{B},k}^{pri}$	$\bar{\alpha}_{2k}$	$v_{\mathbf{A},k}^{post}/v_{\mathbf{A},k}^{pri}$
$\bar{\gamma}_{1k}$	$1/v_{\mathbf{B},k}^{pri}$	$\bar{\gamma}_{2k}$	$1/v_{\mathbf{A},k}^{pri}$
$\bar{\eta}_{1k}$	$1/v_{\mathbf{B},k}^{post}$	$\bar{\eta}_{2k}$	$1/v_{\mathbf{A},k}^{post}$
τ_{1k}	$\tau_{\mathbf{B},k}$	τ_{2k}	$\tau_{\mathbf{A},k}$

for all v_1 , v_2 , and covariance matrices \mathbf{S} . Moreover, the values of the limits are continuous in \mathbf{S} , v_1 , and v_2 .

C.2 Further Clarifications

Although Turbo-CS [21] and VAMP [13, 25] share the same idea, they use different definitions for their variables. This paper adopts the notations used in Turbo-CS. To highlight the equivalence, we summarize in Table 2 the relationship between the SE variables used in this paper and these used in [13]. With this one-to-one correspondence, one can verify the correctness of Theorem 2 by referring to [13], which provides a rigorous proof of SE using VAMP’s notation.

D Training and Inference Details

D.1 Training Configurations

We use the pretrained checkpoint in [30] for the first-order score network. For the second-order score network, we use the same NCSN++ architecture in [30]. It outputs only the diagonal value of the second-order score, yielding the same output dimension as the first-order score network. As suggested by [19], the weighting factor in the training objective (21) is chosen as $\lambda_2(\sigma_i) = 1/\sigma_i^4$. As a side note, for the first-order score matching, the work in [30] uses the weighting factor $\lambda_1(\sigma_i) = 1/\sigma_i^2$, which is consistent with the suggestion in [19]. For the second-order score matching, we adopt the SDE training framework in [30] that applies to continuous noise scales in the range of [0.01, 348]. We use a batch size of 64. The other training parameters are set identically to its first-order counterpart [30]. We train the second-order score network for 1M iterations using 4 NVIDIA A800 GPUs.

Code and checkpoints will be open-sourced upon the acceptance of this paper.

D.2 Inference Configurations

For inference, the proposed method, DPS, and DiffPIR all run on a single NVIDIA A800 GPU. We tune the hyperparameters of the benchmarks as follows:

- DPS [6]: We use 1000 diffusion steps by default. We choose $\rho = 1$ for the best performance. For obtaining the tradeoff curves in Fig. 5, we also test 50, 100, 200, 400 reverse diffusion

Table 3: Quantitative results on FFHQ validation set. The compression ratio is $M/N = 0.4$ and we set $\beta = 0.8$.

Method	$\delta_0 = 0.5$				$\delta_0 = 0.05$			
	PSNR \uparrow	SSIM \uparrow	FID \downarrow	LPIPS \downarrow	PSNR \uparrow	SSIM \uparrow	FID \downarrow	LPIPS \downarrow
STMP (Ours)	24.73	0.7320	61.22	0.0359	33.49	0.9249	31.35	0.0040
DPS	16.75	0.5466	44.89	0.0830	26.66	<u>0.8273</u>	<u>26.46</u>	0.0116
DiffPIR	<u>23.18</u>	<u>0.6461</u>	<u>59.82</u>	<u>0.0464</u>	28.23	0.8100	24.22	<u>0.0081</u>
PnP-ADMM	8.75	0.0381	352.42	0.7221	<u>28.89</u>	0.7530	56.15	0.0118
D-Turbo-CS	8.62	0.0088	372.86	0.8048	24.77	0.5723	117.74	0.0340

Table 4: Quantitative results on FFHQ validation set. The compression ratio is $M/N = 0.7$ and we set $\beta = 1$.

Method	$\delta_0 = 0.5$				$\delta_0 = 0.05$			
	PSNR \uparrow	SSIM \uparrow	FID \downarrow	LPIPS \downarrow	PSNR \uparrow	SSIM \uparrow	FID \downarrow	LPIPS \downarrow
STMP (Ours)	25.82	0.7649	<u>57.76</u>	0.0280	34.98	0.9420	23.42	0.0027
DPS	17.98	0.5888	39.98	0.0653	28.33	<u>0.8596</u>	<u>26.63</u>	<u>0.0081</u>
DiffPIR	<u>24.19</u>	<u>0.7015</u>	86.51	<u>0.0407</u>	28.05	0.7728	27.00	0.0089
PnP-ADMM	8.68	0.0400	341.78	0.7623	<u>29.15</u>	0.7314	43.26	0.0101
D-Turbo-CS	13.92	0.0234	352.49	0.5016	28.04	0.7387	74.22	0.0167

steps.

- DiffPIR [36]: We use 100 diffusion steps by default. We choose $\lambda = 5$ and $\zeta = 1$ for the best performance. For obtaining the tradeoff curves in Fig. 5, we also test 10, 20, 40, 60 reverse diffusion steps.
- PnP-ADMM [4]: We choose the total variation (TV) denoiser for PnP-ADMM. We choose $\lambda = 0.01$, $\rho = 1$, and $\gamma = 1$ for the best performance. The algorithm is executed for 50 iterations.
- D-Turbo-CS [34]: We choose the SURE-LET [3] denoiser for D-Turbo-CS. There is no hyperparameters for D-Turbo-CS. The algorithm is executed for 50 iterations.

E More Results

We provide additional quantitative results in Tables 3 and 4. More recovered images under different compression ratios and noise levels can be found in Figs. 6, 7, and 8.

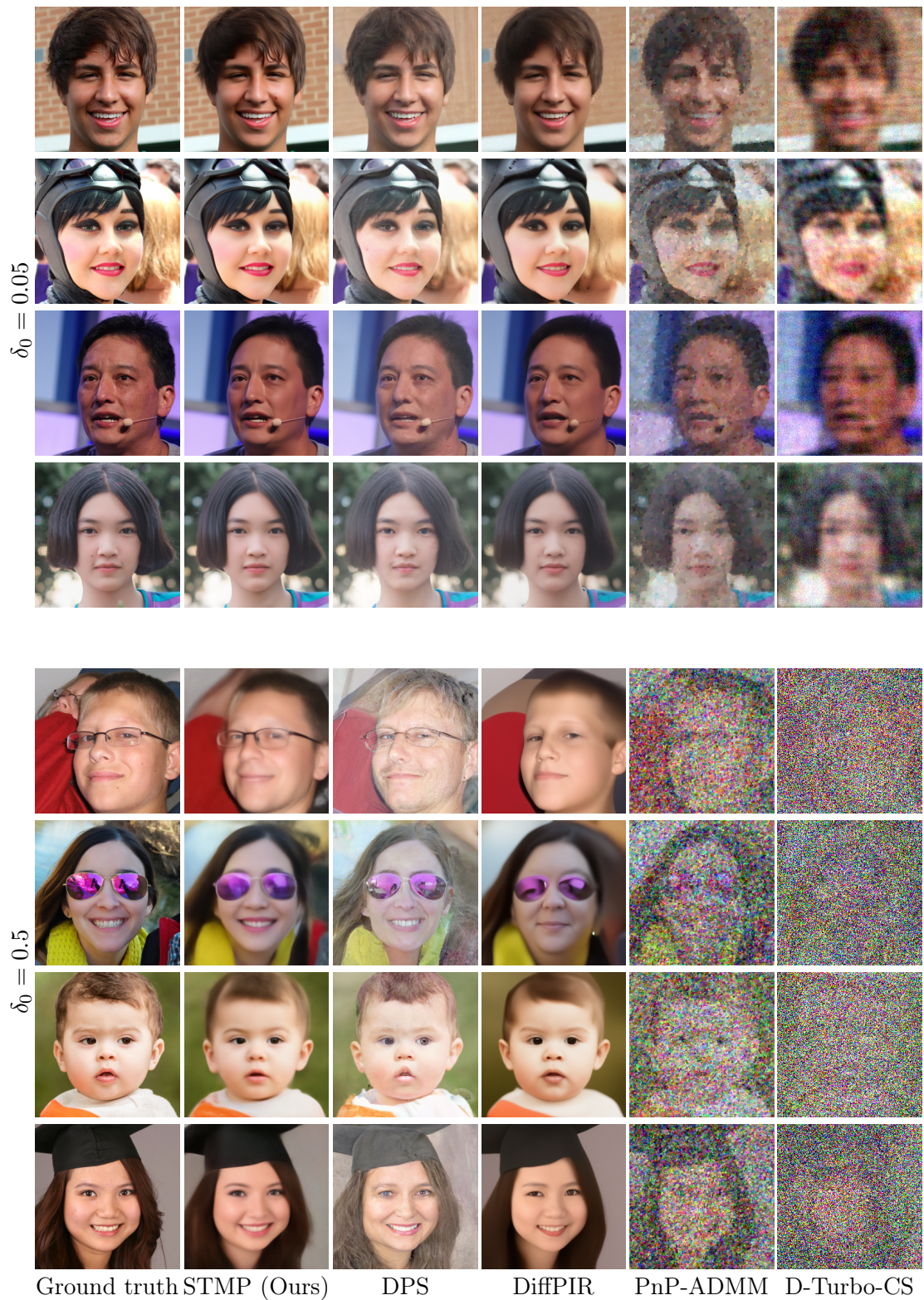


Figure 6: More results on FFHQ validation set. The compression ratio is $M/N = 0.1$ and we set $\beta = 0.5$.

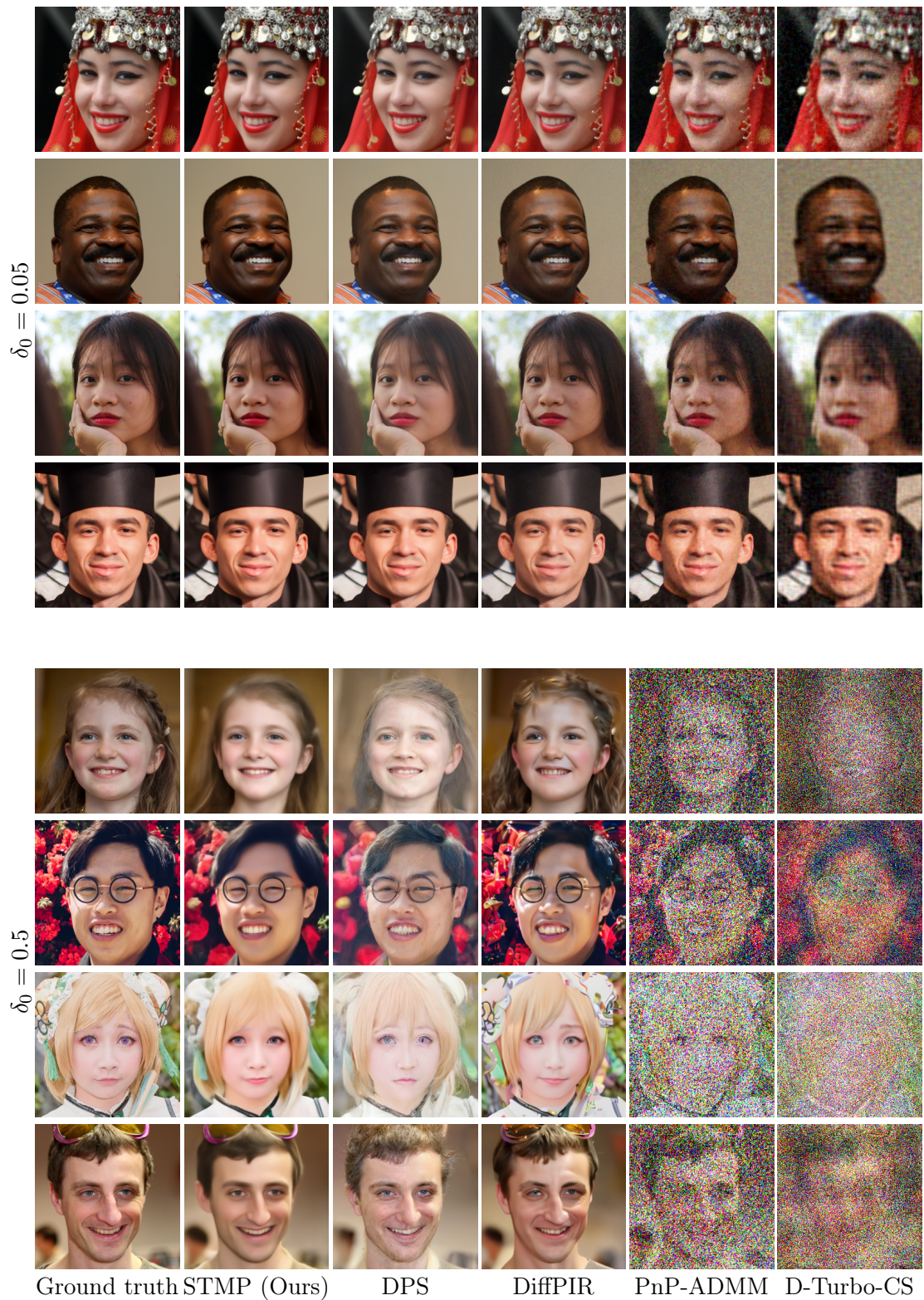


Figure 7: More results on FFHQ validation set. The compression ratio is $M/N = 0.4$ and we set $\beta = 0.8$.

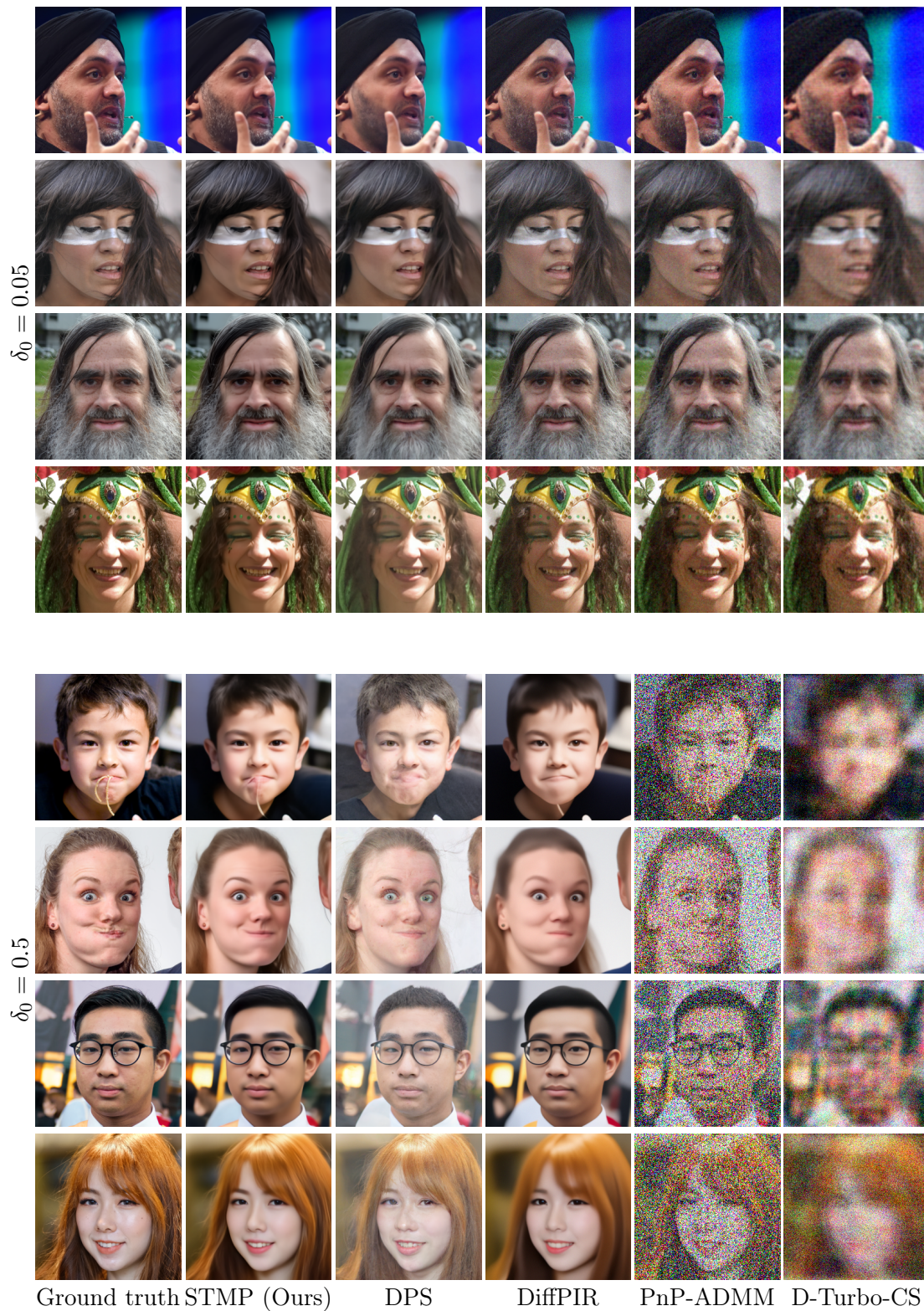


Figure 8: More results on FFHQ validation set. The compression ratio is $M/N = 0.7$ and we set $\beta = 1$.